26.9 A 0.19×0.17mm² Wireless Neural Recording IC for Motor Prediction with Near-Infrared-Based Power and Data Telemetry

Jongyup Lim[1], Eunseong Moon[1], Michael Barrow[1], Samuel R. Nason[1], Paras R. Patel[1], Parag G. Patil[1], Sechang Oh[1], Inhee Lee[1], Hun-Seok Kim[1], Dennis Sylvester[1], David Blaauw[1], Cynthia A. Chestek[1], Jamie Phillips[1], Taekwang Jang[2]

[1]University of Michigan, Ann Arbor, MI
[2]ETH Zürich, Zürich, Switzerland

Brain machine interfaces using neural recording systems [1-4] can enable motor prediction [5-6] for accurate arm and hand control in paralyzed or severely injured individuals. However, implantable systems have historically used wires for data communication and power, increasing risks of tissue damage, infection, and cerebrospinal fluid leakage, rendering these devices unsuitable for long-term implantation (Fig. 26.9.1, top). Recently, several wireless and miniaturized neural recording implants with various power and data transmission methods were proposed. References [7,8] propose an electrocorticography (ECoG) recording system with near-field RF power transfer and bilateral communication, but the 0.5W Tx exceeds maximum exposure limits by 10× [8]. Ultrasonic telemetry can safely send more power than RF; however it requires mm-scale dimensions ($0.8mm^3$ in [9]) due to bulky ultrasound transducers. On the other hand, near infrared (NIR) light can provide power transfer and data downlink via a photovoltaic cell (PV), and a data uplink via a light-emitting diode (LED). Dimensions can be scaled to 100s of microns [10], with [11] demonstrating a $0.0297mm^2$ neural recording system using a $50mW/mm^2$ light source (<1/6th of safety limit for the brain). However, this system is limited to a single channel, and since it only has a surface electrode, it can record only surface potentials (face-down, potentially blocking the light channel) or must itself be injected into brain tissue, creating significant tissue damage and danger of bleeding. In this paper, we propose a 0.74μW, $0.19{\times}0.17mm^2$ IC designed for a wireless neural recording probe. It computes so-called *spiking band power* (SBP) [5,12] on-chip to save 920× power while maintaining accurate finger position and velocity decoding.

A neural probe IC is designed for a larger neural recording system concept (Fig. 26.9.1, bottom) in which numerous micro-probes would be placed on the brain in the sub-dural space to record neural spikes using a carbon fiber electrode that penetrates several mm into brain tissue and has been shown to incur minimal chronic scar formation [13]. The probes will be powered and globally programmed by 850nm NIR light emitted by a *repeater* placed in the epidural space. The LED in the probe will act as the data uplink; its light received by the repeater using a single-photon avalanche diode (SPAD). The repeater would service 100s of probes, which are distinguished by their on-chip ID and location. Given its larger size, the repeater can use an inductive link for wireless power and data communication with an external receiver.

The CMOS IC consists of an optical receiver followed by clock and data recovery, a random-number-generated-based chip ID [14], neural recording amplifier, SBP extractor, and LED driver (Fig. 26.9.2). Figure 26.9.3 shows the schematic and measured signal diagram of the optical receiver (ORx). V_{DD} is AC-coupled to a comparator input to convert modulated light from the repeater to a digital signal. The comparator has 80mV hysteresis to remove glitches due to unwanted V_{DD} fluctuations. In the power-on reset phase, the clock recovery circuit locks the on-chip recovery clock to the precise 8kHz modulated light from the repeater. This is critical since the clock is used to set the reference current, which must be precisely controlled for reliable amplification and signal filtering. The clock recovery circuit searches the digitally-controlled oscillator (DCO) thermometer-coded configurations to match the received modulation period with the DCO period. It then switches the system clock from the default to recovery clock using glitch-free multiplexers. After clock locking, the repeater programs the system using pulse width modulated (PWM) light (downlink). An 8b hardwired passcode is implemented to prevent unwanted programming. The signal diagrams in Fig. 26.9.3 are measured from the proposed chip, wire-bonded with a custom dual-junction GaAs PV cell that generates 893nA I_{SC} and 1.67V V_{OC} under $120.5μW/mm^2$ 850nm light.

The AFE is specifically designed to support SBP [5] based finger position / velocity decoding. SBP is the absolute average of signal amplitude in the 300-to-1000Hz band. When used as input to a trained linear decoding filter, SBP maintains finger position / velocity decoding accuracy relative to a standard 7.5kHz bandwidth neural recording while reducing the required communication bandwidth from probe to repeater to only 100s of Hz, thereby reducing uplink power. The AFE is composed of a three-stage bandpass differential amplifier chain with subsequent source follower and rectifier-based integrator to quantize the SBP (Fig. 26.9.4 left). The LNA, with 60MΩ input impedance at 1kHz, is fully differential and achieves 30dB gain without bulky capacitors by implementing its gain using g_m ratio. VGA1 and VGA2 set the high-cut-off (f_H, 950Hz) and low-cut-off frequencies (f_L, 180Hz), respectively, and define the spiking band. f_H is set by VGA2 bias current, which is generated by a current reference implemented using a voltage reference and switched capacitor operating at f_{CLK}. f_L is defined by the VGA2 DC servo loop, whose feedback impedance is defined by $1/C_{SW}f_{CLK}$. Accuracy of f_H and f_L is ensured by locking f_{CLK} during clock recovery to the repeater. Peak gain is measured at 69dB while amplifying action potential (AP) spikes in 180–950Hz bandwidth for SBP-based motor prediction. Measured input-referred noise (IRN) is 4.8μVrms while consuming 510nW at 38°C.

The 3-stage amplifier drives a rectifier (Fig. 26.9.4 bottom left) whose output is initially precharged to $VREF_H$. The rectifier output decays at a rate proportional to its input amplitude. When it drops below $VREF_L$, a pulse is generated on LED_EN. This triggers the LED driver to transmit a Manchester encoded (unique) chipID (Fig. 26.9.5 top left) consuming 6.7pJ/bit (post layout simulation). Therefore, the LED firing rate or frequency is proportional to the SBP. AFE functionality was also verified *in vivo* using a carbon fiber driven ~1.3mm into the motor cortex of an anesthetized Long Evans rat. A commercial recording system (24.414kSps, [2.2Hz, 7.5kHz] BW) is connected to the carbon fiber electrode in parallel to the IC for accuracy comparison. All procedures complied with the Institutional Animal Care and Use Committee. VIN is the input of the proposed amplifier, measured by the high-power commercial recording system. VOUT($VOUT_P$-$VOUT_N$) is the amplifier measured output. Results show that the rectifier output (INTOUT) steps down at each motor cortex neuron spike and is restored to $VREF_H$ when it reaches $VREF_L$ (Fig. 26.9.4).

LED firing rate linearity across SBP is tested using synthesized AP spikes ($240μV_{pk\text{-}to\text{-}pk}$, 1ms width) with varying rates from 0 to 100Hz (Fig. 26.9.5 top right). The measured LED firing rate is proportional to SBP with nonlinearity <2.9% and its sensitivity is programmable from 0.4 to 5.0 firings per μV. Overall functionality is verified using three different types of input signals; synthesized neural simulator, *in vivo* rat motor cortex, and pre-recorded monkey motor cortex (Fig. 26.9.5 bottom). Measured probe SBP is decoded from the measured time interval of LED_EN signal and compared with the result generated by a conventional high-power analog front-end and DSP SBP calculation [5]. The measured probe SBP accurately matches the conventional system results. Figure 26.9.6 (top) shows finger position / velocity decoding results using Kalman-Filter (KF) [6] with conventional and probe SBP from pre-recorded 20-channel neural signals of a male monkey. All procedures complied with the Institutional Animal Care and Use Committee. The system accurately predicts finger position / velocity with state-of-the-art correlation coefficient of 0.8587 / 0.5919 while a conventional high-power and wired system demonstrates 0.8886 / 0.6155 correlation coefficient. The IC is fabricated in 180nm CMOS (Fig. 26.9.7). Figure 26.9.6 (bottom) compares to previously published wireless neural probe chip designs. It consumes 0.74μW with 3.76 amplifier NEF at 1.5V supply and 38°C, achieving best noise performance among comparable designs [7,9,11].

Acknowledgements:
This work is supported by the NIH (1R21EY029452-01).

References:

[1] C.M. Lopez et al., "22.7 A 966-Electrode Neural Probe with 384 Configurable Channels in 0.13μm SOI CMOS," *ISSCC*, pp. 392-393, Feb. 2016.
[2] B.C. Johnson et al., "An Implantable 700μW 64-Channel Neuromodulation IC for Simultaneous Recording and Stimulation with Rapid Artifact Recovery," *IEEE Symp. VLSI Circuits*, pp. C48-C49, 2017.
[3] H. Chandrakumar and D. Markovic, "27.1 A 2.8μW 80mVpp-Linear-Input-Range 1.6GΩ-Input Impedance Bio-Signal Chopper Amplifier Tolerant to Common-Mode Interference up to 650mVpp," *ISSCC*, pp. 448–449, Feb. 2017.
[4] C. Kim et al., "A 92dB Dynamic Range Sub-μVrms-Noise 0.8μW/ch Neural-Recording ADC Array with Predictive Digital Autoranging," *ISSCC*, pp. 470–471, Feb. 2018.
[5] Z. T. Irwin et al., "Enabling Low-Power, Multi-Modal Neural Interfaces Through a Common, Low-Bandwidth Feature Space," *IEEE TNSRE*, vol. 24, no. 5, pp. 521–531, May 2016.

978-1-7281-3205-1/20/$31.00 ©2020 IEEE
Authorized licensed use limited to: University of Michigan Library. Downloaded on June 02,2020 at 13:46:37 UTC from IEEE Xplore. Restrictions apply.

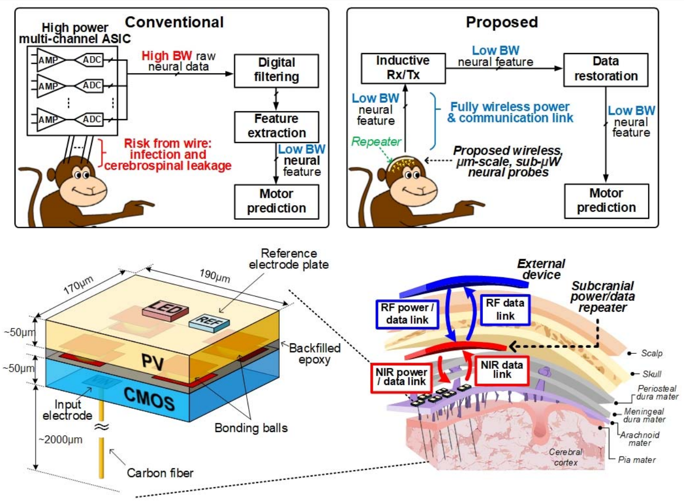

Figure 26.9.1: Conventional and proposed neural recording system (top); concept diagram of proposed neural probe and two-step approach for recording and transmitting neural signals (bottom).

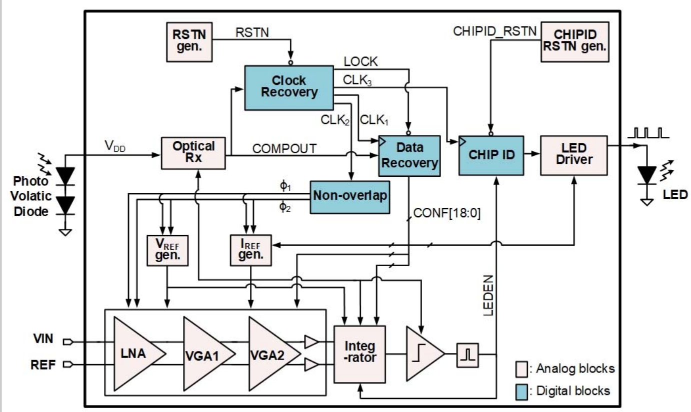

Figure 26.9.2: Top-level circuit diagram of the neural recorder.

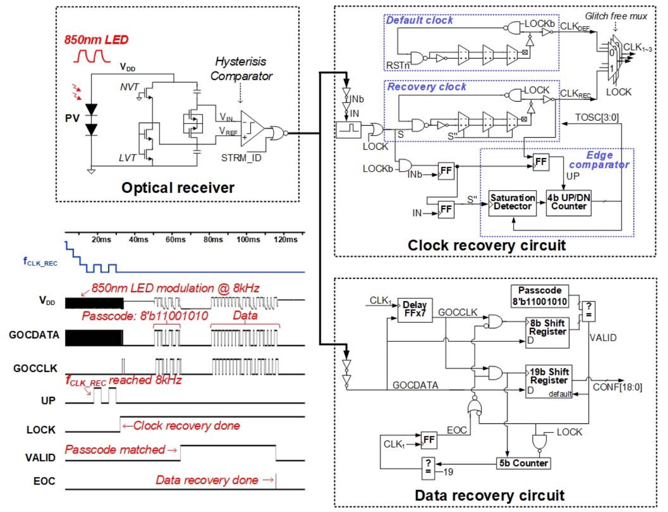

Figure 26.9.3: Optical receiver (top left), clock recovery circuit (top right), data recovery structure (bottom right), and measured signal diagram during clock and data recovery (bottom left).

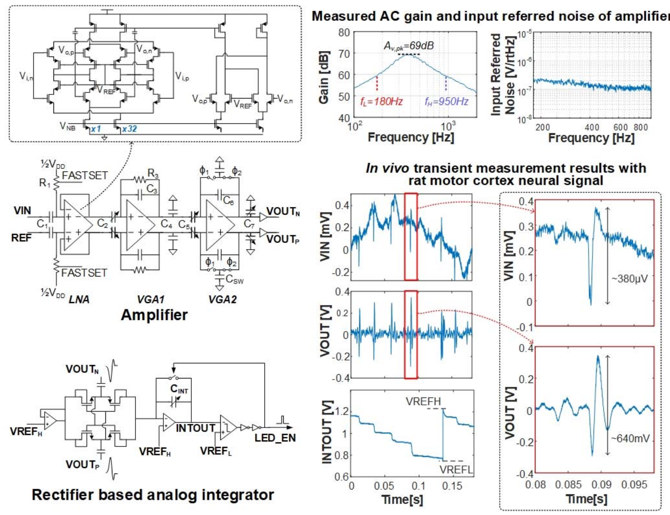

Figure 26.9.4: Amplifier (top left), rectifier based analog integrator (bottom left), measured amplifier AC and noise performance (top right), *in vivo* measurement results from a motor cortex of rat (bottom right).

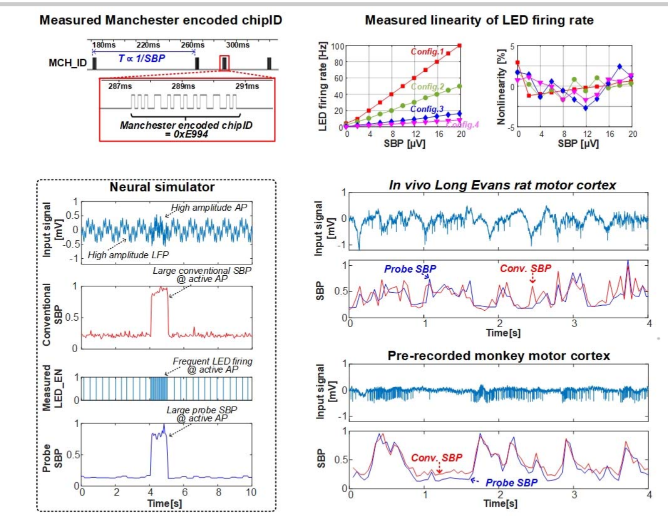

Figure 26.9.5: Measured timing diagram of Manchester encoded chip ID (top left), measured linearity of LED firing rate across SBP (top right), and measured transient waveform from three types of input neural signals (bottom).

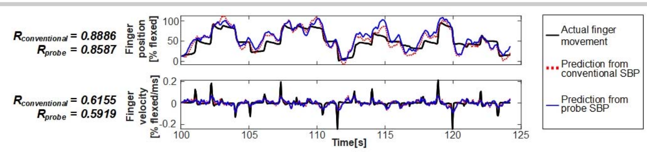

		This work	NER 2019 [7]	ISSCC 2019 [9]	ISSCC 2018 [11]
Technology [nm]		180	65	65	180
Wireless power source		Optical	RF	Ultrasonic	Optical
Data transimmision method		Optical	RF	Ultrasonic	Optical
Data transimmision	Up-link	SIM (Symbol Interval Modulation)	BPSK-modulated RF backscatter	AM backscatter	PPM
	Down-link	PWM	ASK-PWM	No	No
On-chip feature extraction		SBP	No	No	No
Chip ID		16b	24b	No	No
Clock recovery		Yes	No	No	No
Supply [V]		1.5	0.6	1	0.9
Power [µW]	Total	0.74	40	28.8	< 1
	Amplifier	0.51	3.2	4	< 0.52
Area [mm²] (W [mm] x L [mm])		0.0323 (0.19 x 0.17)	0.25 (0.5 x 0.5)	PZT: 0.5625 (0.75 x 0.75) IC :0.25 (0.5 x 0.5)	0.0297 (0.330 x 0.090)
Target neural signal		AP	ECoG (epicortical)	LFP, AP	LFP, AP
Gain[dB]		69	N/A	24	24
Bandwidth[Hz]		180 ~ 950*	500	5000	10000
Input referred noise [µVrms]		4.8†	2.2	5.3	42
NEF		3.76	8.7	5.87	12.3

* -10dB cutoff frequency
† Output noise divided by transfer function

Figure 26.9.6: Finger position / velocity decoding result using KF with the probe and conventional SBP with pre-recorded 20-channel neural signals of a monkey (top) and comparison table (bottom).

26

Authorized licensed use limited to: University of Michigan Library. Downloaded on June 02,2020 at 13:46:37 UTC from IEEE Xplore. Restrictions apply.

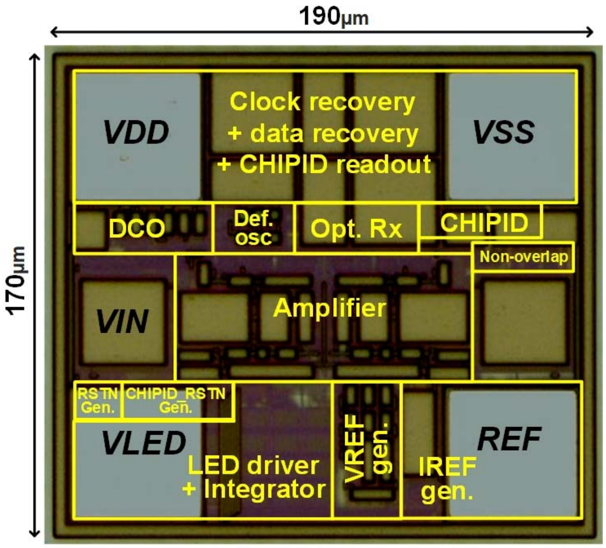

Figure 26.9.7: Die photo of the IC in 180nm CMOS.

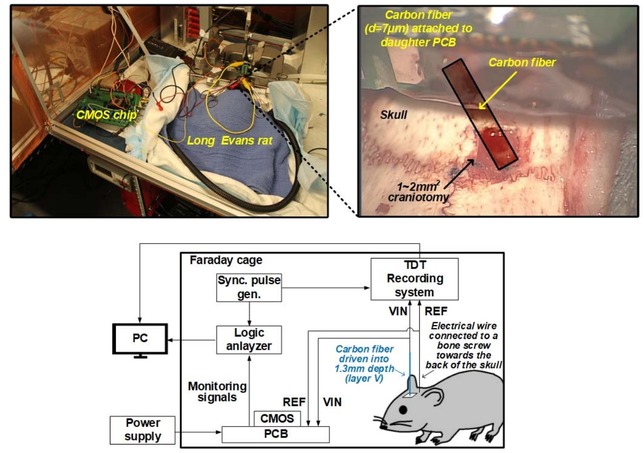

Figure 26.9.S1: Photo of *in vivo* testing setup (top left). Carbon fiber mounted to PCB is inserted (top right) and a bone screw was placed at the most posterior portion of the skull. Recordings were taken with the IC in parallel with RA16AC headstage, RA16PA pre-amplifier, and RX7 Pentusa base station (Tucker-Davis Technologies, Alachua, FL, 2.2-7500Hz bandpass filtered) (bottom).

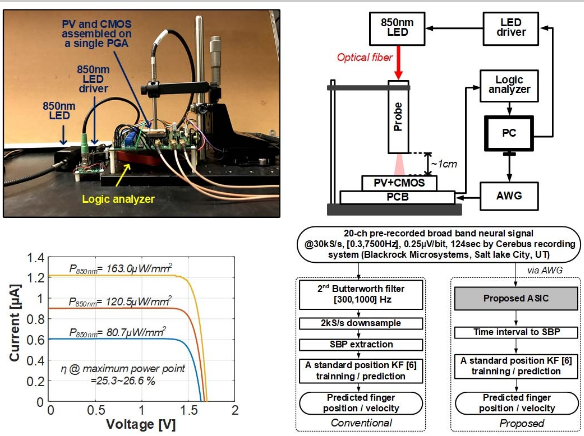

Figure 26.9.S2: Optical setup with the IC wire-bonded with a custom dual-junction GaAs PV (top), measured performance of the PV (bottom left), and flow chart of finger position and velocity decoding (bottom, right). Pre-recorded neural signal from the motor cortex of a rhesus macaque and one-dimensional aperture of fingers at 1kHz during a finger-based target acquisition task are used.

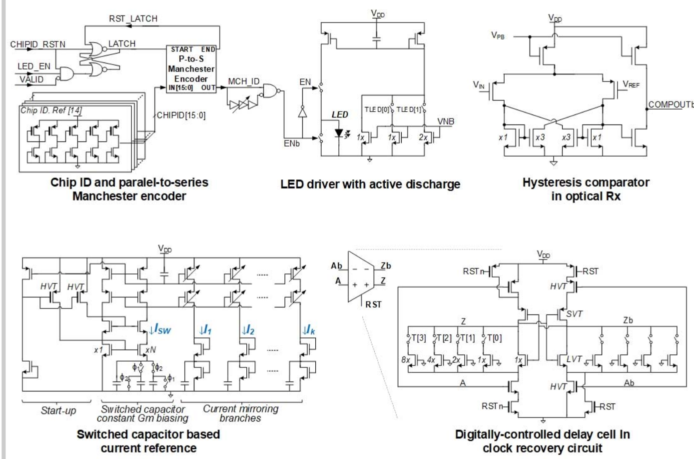

Figure 26.9.S3: Structure of chip ID and readout circuit (top left), current sourcing based LED driver with active discharge (top middle), comparator with hysteresis (top right), switched capacitor based current reference (bottom left), and leakage based DCO delay cell (bottom right).

Additional References:

[6] Z. T. Irwin et al., "Neural Control of Finger Movement via Intracortical Brain-Machine Interface," *J. Neural Engineering*, vol. 14, no. 6, p. 066004, Dec. 2017.

[7] J. Lee et al., "An Implantable Wireless Network of Distributed Microscale Sensors for Neural Applications," *Int. IEEE/EMBS NER*, pp.871-874, 2019.

[8] J. Lee et al., "Wireless Power and Data Link for Ensembles of Sub-mm scale Implantable Sensors near 1GHz," *IEEE BioCAS*, pp.1-4, 2018.

[9] M.M. Ghanbari et al., "A 0.8mm² Ultrasonic Implantable Wireless Neural Recording System with Linear AM Backscattering," *ISSCC,* pp. 284-285, Feb. 2019.

[10] X. Wu et al., "A 0.04mm³ 16nW Wireless and Batteryless Sensor System with Integrated Cortex-M0+ Processor and Optical Communication for Cellular Temperature Measurement," *IEEE Symp. VLSI Circuits,* pp. C191-C192, 2018.

[11] S. Lee et al., "A 330μm×90μm Opto-Electronically Integrated Wireless System-on-Chip for Recording of Neural Activities," *ISSCC,* pp. 292-293, Feb. 2018.

[12] E. Stark, and M. Abeles, "Predicting Movement from Multiunit Activity," *J. Neurosci.*, vol. 27, no. 31, pp. 8387-8394, Aug. 2007.

[13] P. R. Patel et al., "Chronic In Vivo Stability Assessment of Carbon Fiber Microelectrode Arrays," *J. Neural Engineering,* vol. 13, no. 6, p. 066002, Dec. 2016.

[14] K. Yang et al., "A 553F² 2-Transistor Amplifier-Based Physically Unclonable Function (PUF) with 1.67% Native Instability," *ISSCC,* pp.146-147, Feb. 2017.

 978-1-7281-3205-1/20/$31.00 ©2020 IEEE

Authorized licensed use limited to: University of Michigan Library. Downloaded on June 02,2020 at 13:46:37 UTC from IEEE Xplore. Restrictions apply.